

Energy Efficiency Modeling for Configuration-Dependent Machining via Machine Learning: A Comparative Study

Qinge Xiao, *Member, IEEE*, Congbo Li[✉], *Senior Member, IEEE*, Ying Tang, *Senior Member, IEEE*, and Xingzheng Chen, *Member, IEEE*

Abstract—Energy efficiency modeling is of great importance to energy management and conservation for machinery enterprises. To improve the generalization ability, this article combines the machining parameters and the configuration parameters into energy efficiency models, for which machine-learning (ML) algorithms are used considering the lack of theoretical formulas. Based on the three-year data collected in a shop floor, a comparative study for two different cases is conducted with a particular focus on prediction accuracy, stability, and computational efficiency. In Case 1, only cross-sectional data are used to predict energy efficiency, ignoring the deterioration of spindle motors and cutting tools. Three traditional ML algorithms, i.e., artificial neural networks, support vector regression, and Gaussian process regression, are evaluated with the help of five error metrics. In Case 2, we construct the models in a more realistic situation that considers the dynamic aspects of spindle motor aging and tool wear. A convolutional neural network, a stacked autoencoder, a deep belief network and the aforementioned traditional ML algorithms are investigated. The comparison shows that all the models in Case 1 suffer from performance degradation, while deep learning achieves the long-term improvement in accuracy.

Note to Practitioners—Energy efficiency models deliver many advantages, ranging from energy-aware machine design to process optimization. Although a large amount of works in the past focused on physics-based and experimental modeling for specific machining configurations, it can be more effective to improve the applicability of the modeling methods by involv-

Manuscript received June 4, 2019; revised September 5, 2019 and November 7, 2019; accepted December 16, 2019. Date of publication January 14, 2020; date of current version April 7, 2021. This article was recommended for publication by Associate Editor Y. Liu and Editor F.-T. Cheng upon evaluation of the reviewers' comments. This work was supported in part by the National Natural Science Foundation of China under Grant 51975075, in part by the National Key Research and Development Program of China under Grant 2019YFB1706103, and in part by the Fundamental Research Funds for the Central Universities of China under Grant cqu2018CDHB1B07. (*Corresponding author: Congbo Li*.)

Qinge Xiao and Congbo Li are with the State Key Laboratory of Mechanical Transmission, Chongqing University, Chongqing 400044, China (e-mail: xqg2974@163.com; congbo@cqu.edu.cn).

Ying Tang is with the Department of Electrical and Computer Engineering, Rowan University, Glassboro, NJ 08028 USA, and also with the Institute of Intelligent Manufacturing, Qingdao Academy of Intelligent Industries, Qingdao 266000, China (e-mail: tang@rowan.edu).

Xingzheng Chen is with the College of Engineering and Technology, Southwest University, Chongqing 400715, China (e-mail: chenxingzheng233@163.com).

Color versions of one or more of the figures in this article are available online at <https://ieeexplore.ieee.org>.

Digital Object Identifier 10.1109/TASE.2019.2961714

ing the configuration variables into the models. Due to the uncertainties in both the machine and the operation environment, machine learning is adopted to fit the high-dimensional and high-nonlinearity energy system. To the best of our knowledge, this is the first article that provides a comprehensive survey on ML-based modeling in terms of data sizes, temporal granularities, feature selection, and algorithm performance. Such a survey helps engineers quickly justify the appropriate ML methods to meet the actual requirements.

Index Terms—Deep learning (DL), energy efficiency modeling, machine-learning (ML), machining system.

I. INTRODUCTION

ENERGY demand, excepted to rise to 47% over the next 15 years, is increasing dramatically in accordance with the population growth and industrialization [1]. The industrial manufacturing sector is by far the biggest electrical energy consumer with a share of more than 30% of the global total [2]. Many attempts are being made worldwide to decrease the energy usage in the manufacturing process, among which strategies associated with machine tools, such as launching EU directives for ecodesign and initiating ISO 14995 for energy measurement, are the most prominent [3]. Energy efficiency is a measure for achieving energy conservation [4]. Energy (efficiency) modeling of machine tools helps to evaluate the energy efficiency in different machining conditions or when different machining parameters are adopted, providing a useful tool of investigating the energy mechanism [5]. As a precondition for energy-aware design and optimization, energy (efficiency) modeling has received sustained attention in the past couple of decades [6].

The existing modeling methods can fall into two categories: physical methods and experimental statistical methods. Physical modeling is a kind of white-box technique, where energy efficiency models are established based on the principles of energy transferring from electrical systems to mechanical systems. However, due to the nondeterministic and process-dependent nature of mechanical machining, physical models are less practical [7]. Experimental statistical methods are much preferred in this domain, especially when lacking of physical basis [8]. In these methods, experiments are first conducted by varying the machining parameter combinations under various machine-tool-workpiece conditions. Based on

the experimental energy data, the mapping relationships are explored through statistical methods such as polynomial regression [9] and ridge regression [10].

It is worth mentioning that although the physical and experimental methods are widely used for machining practice, they are in general developed toward specific machining configurations, where parameter spaces, machine tool specifications, and tool-workpiece combinations are predetermined. Due to the lack of the consideration of the configuration parameters (e.g., machine tools, cutting tools, and workpieces) in the energy efficiency models, it is insufficient to predict energy efficiency for these interactive and integrated machining systems [5]. Yet, when any change occurs to the configurations, a new round of modeling should be performed all over again. The sacrifice of computational efficiency becomes more prominent for flexible machining where frequent alterations in machining configurations can be usually observed [11], [12]. In this context, new challenges arise when developing the generalized models of energy efficiency with the consideration of complex chip formation, material property requirements, tool wear, machine degradation, and so on.

On the other hand, the increase in the dimension of the configuration parameters usually means higher computational complexity of modeling. However, when fitting high-nonlinear and high-dimensional functions, there might be problems of multicollinearity and numerical instability facing classical statistical methods, bringing about a negative influence on prediction ability [8]. Machine-learning (ML) techniques make it possible to turn the huge amount of machinery data into actionable information even facing complicated behaviors [13]. ML tools have been broadly investigated in scientific studies, offering new alternatives for the modeling of the machining systems. Examples of the approaches are found in research, such as artificial neural networks (ANNs) [14], support vector regression (SVR) [15], Gaussian process regression (GPR) [16], and regression trees (RTs) [17]. However, applications of ML algorithms for energy modeling are yet limited, which can be divided into three groups. Majority of the works studied parameter-dependent ANN models. Exemplification can be found in [18] and [19]. The second line of research built energy models with a partial consideration of the machining configuration variables. For instance, Quintana *et al.* [20] developed an ANN predictor to model power consumption in high-speed ball-end milling operations using machining parameters, tool radius, and lubrication as inputs. Al-Hazza *et al.* [21] incorporated tool rake into the ANN model for predicting energy consumed in high-speed hard-turning. A third line of research sought to apply other approaches such as GPR [22] and its variation [23] to improve the accuracy of the ANN models. In recent years, deep learning (DL), as a main batch of ML, has witnessed an overwhelming success in audio recognition [24], computer vision [25], and natural language processing [26]. DL tools have frequently broken new records of accuracy in a large amount of applications. It is then a natural practice to apply the DL models for machining systems to enhance the prediction performance. Although there are few references related to DL-based energy efficiency modeling, DL techniques have

been tested with good performance in other related areas, such as machinery fault diagnosis [27], tool wear [28], and machine remaining life prediction [29].

ML models have gained a lot of research attention, and in response, a number of survey studies focusing on the comparative analysis of the existing ML approaches have been published. The focus of Pimenov *et al.* [30] was on the performance comparison of a series of ML methods (i.e., random forest, multilayer perceptions, RTs, and radial-based functions) in cutting power prediction. A similar work studying the ANN and SVR methods for the prediction of roughness, cutting force, and tool life can be found in [31]. Those comparative studies are essential to offer insights in terms of the research potential of ML-based modeling for the machining systems and current research gaps [32]. Nonetheless, there is a lack in survey studies that look into the ML-based models in predicting machining energy efficiency, particularly in terms of the types of data (e.g., simulated data, monitoring data, and derived data), the types of features (e.g., machining parameters and machining configuration variables), and the sizes of the data (e.g., interval of data collection and the amount of data instances). Filling this research gap is the objective of this article. More specifically, this article studies three traditional ML algorithms (i.e., ANN, SVR, and GPR) and three typical DL algorithms [i.e., convolutional neural network (CNN), stacked autoencoder (SAE), and deep belief network (DBN)], as well as their performance in machining efficiency prediction. To sum up, readers can benefit from the comparative study in the following aspects.

1) We investigate the ML methods from a more multivariate perspective such as feature selection, data size, and collection interval for energy efficiency modeling. With such an investigation, it becomes easier for readers to identify the appropriate methods according to the available data set.

2) We derive general and useful tips for the design of ML models (both traditional ML models and DL models). The neural network structure and algorithm parameters provided in this article help readers to expand them in a specific application.

The rest of this article is organized as follows. The study context including problem description and challenges of the configuration-dependent energy efficiency modeling is described in Section II. The primary works for energy efficiency modeling such as identifying model inputs, research methodology, and evaluation indexes are introduced in Section III. Machinery data acquisition, data preprocessing, and data set design are detailed in Section IV. Modeling processes and results for cases under different scenarios are discussed in Section V, followed by the concluding remarks in Section VI.

II. PROBLEM STATEMENT

In this section, we present the preliminary background for energy efficiency modeling. First, the configuration parameters in the machining system are illustrated in Section II-A. The particular challenges associated with the consideration of configuration parameters in energy efficiency modeling are then discussed in Section II-B.

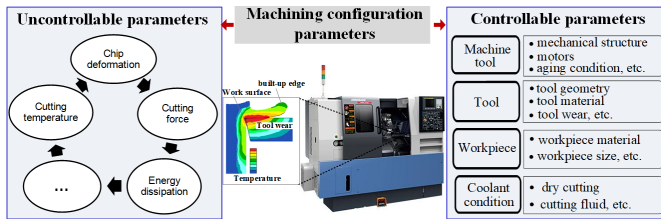


Fig. 1. Machining configuration variables in machining operations.

A. Configuration Parameters in Machining System

Machining configuration characterizes the physical environment, where operations are conducted after making a sequence of decisions of equipment and machining parameters. In reality, machining configuration should be first clarified according to the selection principle at the hardware level, based on which proper machining parameters such as cutting speed, feed rate, and depth of cut are systematically set with the constraints of machining configuration. Machining configuration parameters can be generally divided into two categories, controllable parameters and uncontrollable parameters, as summarized in Fig. 1.

Controllable parameters, as the name indicates, are the ones that can be selectively determined for a machining operation. Typical controllable parameters are machine tools, cutting tools, workpieces, and coolant condition. Despite the controllable parameters that are relatively independent of the machining processes, coordination of these parameters is always required based on the consideration of the processing needs and system rigidity.

Uncontrollable parameters commonly refer to the parameters that are specified as not optional. Such parameters are not readily available before process initiation but only can be observed during machining. The parameters such as cutting force, temperature, workpiece deformation, and energy dissipation are the major concerns in the machining processes due to their critical influence on the quality and cost of part manufacturing.

B. Necessity and Challenges of Energy Efficiency Modeling for Configuration-Dependent Machining System

With the advancement of numerical control (NC) programming, modern machining becomes more adaptable and flexible. The generalization ability of the models in predicting energy efficiency is much needed to keep up with the rapid development, especially when the machining configuration is frequently changed. However, the current approaches usually model energy efficiency modeling under a specific machining configuration as $\eta_{\partial_i}(x)_{i=1,2,\dots}$, where η is the energy efficiency model, ∂_i is the i th configuration, and x represents the corresponding machining parameters. This article attempts to address the issue by developing a comprehensive model $\eta(\partial_1, \partial_2, \dots, x)$ that can be generalized to various configurations. Learning from the data collected in a daily basis, the constructed model with high prediction accuracy helps to facilitate evaluating energy efficiency for a target operation more efficiently.

The configuration parameters impose a challenging issue on energy efficiency modeling, which can be understood in two aspects: 1) machining system is a mix-attribution system, where configuration parameters possess both continuous attributes (e.g., workpiece diameter) and categorical attributes (e.g., workpiece material) and 2) these mix-attribution parameters coexist in the machining processes with strong interaction effects, making it difficult to describe a theoretical model for such complex systems [33]. ML does not perform theoretical analysis. Instead, it tries to treat the machining system as a black-box and learns patterns from available data. The application of ML for energy efficiency prediction will be elaborated in Sections III–V.

III. ENERGY EFFICIENCY MODELING

A. Definition of Energy Efficiency

Energy utilization ratio and specific energy consumption are two commonly used energy efficiency indexes [34]. In this article, energy utilization ratio that qualifies the conversion rate of the total energy intake to produce energy output is considered as the target object for modeling. The definition of η is given in the following equation:

$$\eta = \frac{E_{\text{mr}}}{E_{\text{total}}} \in [0, 1] \quad (1)$$

where E_{mr} denotes the material removal energy that represents the output of the machining system and E_{total} denotes the total energy consumption that represents the input of the machining system and can be calculated as a sum of standby energy (E_{st}), unload energy (E_u), material removal energy (E_{mr}), additional load loss (E_{ad}), and auxiliary system energy (E_{auc})

$$E_{\text{total}} = E_{\text{st}} + E_u + E_{\text{mr}} + E_{\text{ad}} + E_{\text{auc}}. \quad (2)$$

B. Model Inputs

There are numerous configuration parameters in mechanical machining, and thus, clarifying the critical parameters that effect energy consumption becomes a priority for energy efficiency modeling. This section discusses the determination of inputs in the energy model with a characteristic analysis from the energy decomposition viewpoint.

1) *Standby Energy (E_{st})*: E_{st} refers to the basic energy that exists from the beginning to the end of the operations. Energy consumption by both the functional devices and the peripheral devices is included in this element. Thus, the selection of machine tools has a significant impact on the standby energy. In addition, the machining configuration parameters like the cutting length or the air-cutting length that affect the processing time would also influence it.

2) *Unload Energy (E_u)*: E_u denotes the energy consumed by rotating the spindle and control of the feed drive systems without cutting. As indicated in [34], the overwhelming majorities of these energy losses contribute to the heat generations of the spindle and feed motors. Hence, besides machine specification, spindle motor temperature that reflects the aging condition should also be considered as the influential configuration parameters for the unload energy.

3) *Material Removal Energy (E_{mr})*: E_{mr} refers to the energy consumption that governs chip formation and surface generation. Since this element originates from the cutting force, E_{mr} contains information on workpiece conditions (i.e., material and heat treatments) and tool conditions (i.e., tool geometries, tool wear, and tool material). Given that the cooling in the form of water solution has found little effect on the material removal energy [12], the impact of coolant condition can be ignored.

4) *Additional Load Loss (E_{ad})*: E_{ad} concerns the variable energy loss in the spindle motor and the mechanical transmission systems during the material removal process [8]. Our previous study has found that additional load loss is a quadratic function of the material removal power, so that what affects E_{mr} in turn affects E_{ad} . The investigation shows that the coefficients of the quadratic function are tightly associated with machine specification. Therefore, from the machining configuration perspectives, the additional load energy loss is related to workpieces, tools, and machine specifications.

5) *Auxiliary System Energy (E_{auc})*: E_{auc} is produced by the electric consumers of the cutting-related auxiliary systems. As a part of the machine tool, the energy consumption of these systems is dependent on machine specification. In the processing state, some of the systems, such as the spindle cooling pump and the heat exchanger, are always running, while others are switched on or off according to the machining configuration [35]. For instance, the running status of the cutting fluid system is based on the coolant condition.

Energy modeling for a configuration-dependent machining system is a complex multi-input, multicoupling, and high nonlinear problem. As our interest is to construct an energy-efficiency model, the configuration and machining parameters are selected as the input variables that include $X = \{x_i\}_{i=1,2,\dots,15}$, where x_1 is the cutting speed (v_c), x_2 is the feed rate (f_r), x_3 is the cutting depth (a_p), x_4 is the machine (m_t), x_5 is the tool rake (t_r), x_6 is the edge angle (t_e), x_7 is the tool material (t_m), x_8 is the diameter of the workpiece (w_d), x_9 is the cutting length (w_c), x_{10} is the air-cutting length (w_a), x_{11} is the material of the workpiece (w_m), x_{12} is the heat treatments (w_h), x_{13} is the coolant condition (c_o), x_{14} is the motor temperature (m_o), and x_{15} is the tool wear (t_w).

C. Methodology

In order to figure out the techniques presenting the best prediction performance under different scenarios, three traditional ML methods and three DL methods are chosen due to their extensive use in prediction modeling. Each one is briefly reviewed in the following section.

1) *ANN*: An ANN is a typical ML modeling technique inspired by the human central nervous system. An ANN model typically consists of three layers with different neurons, i.e., input layer, hidden layer(s), and output layer. The neurons in separate layers are interconnected to transmit and deduce information. The computing mechanism of a typical three-layer ANN is as follows: the data collected from the real world are first fed into the input layer. In the hidden layer, the net input is then computed through a sum of multiplications of x with the relevant weights and a suitable activation function.

Finally, the hidden neurons are connected to the output layer, where the outputs are weighted and then summed up in the output neuron. Accordingly, we present the mathematical form of an ANN as

$$y = f(x) = \sum_{j=1}^J (w_j \delta \left(\sum_{i=1}^I w_{ij} x_i + b_j \right)) + \beta + \varepsilon \quad (3)$$

where x is an I -dimensional input vector, w_{ij} is the weight factor connecting the i th input neuron and the j th hidden neuron, b_j is the bias for the j th hidden neuron, w_j is the weight factor connecting the j th hidden neuron and the output neuron, β is the bias for the output neuron, and ε is a random error.

2) *GPR*: GPR is a nonparametric Bayesian modeling technique that assumes that the regression function has a Gaussian prior distribution $f(x) \sim \text{GP}(0, \Sigma(x))$, where $\Sigma(x)$ is the covariance characterized by a positive-definite kernel function $\Sigma_{ij} = K(x_i, x_j)$. The predictive performance relies exclusively on the suitability of the selected kernel [37]. For the noisy observations, a widely used squared-exponential (SE) kernel is given by

$$K(x_p, x_q) = \mu^2 \exp \left(-\frac{1}{2\ell^2} (x_p - x_q)^2 \right) + \vartheta^2 \delta_{pq} \quad (4)$$

where ℓ is the length scale over which the function changes, μ^2 controls the vertical scale of the function, ϑ^2 is the noise variance, and parameter $\delta_{pq} = 1$ if $q = p$; otherwise, $\delta_{pq} = 0$.

The hyperparameter set $\theta = (\ell, \mu, \vartheta)$ of the GPR model can be estimated through an empirical Bayes approach by maximizing the marginal likelihood function, as shown in (5). Readers are referred to [38] for more details

$$L(\theta) = -\frac{N}{2} \log(2\pi) - \frac{1}{2} \log(\det(K)) - \frac{1}{2} y^T K^{-1} y. \quad (5)$$

3) *SVR*: It is developed based on the concept of support vector classification, which attempts to minimize the training error and a confidence interval by finding the hyperplane to separate the training data optimally. SVR is a kernel-based ML method, where kernel functions are adopted to map the input space into a higher dimensional feature space. In a similar fashion of Gaussian processes (GPs), the prediction calculated by an SVR machine for a test case x with N samples is given by (6). The detailed derivation process can be found in [31]

$$f(x) = \sum_{i=1}^N (\alpha_i^* - \alpha_i) K(x_i, x_j) + b \quad (6)$$

where α_i^*, α_i are the Lagrangian multipliers, $K(x_i, x_j)$ is a kernel function, x_i and x_j are the different samples, and b is the unknown coefficient. Radial basis function (RBF) is a commonly used kernel function, and it is calculated as

$$K(x_p, x_q) = \exp \left(-\frac{\|x_p - x_q\|^2}{2\sigma^2} \right) = \exp(-\gamma \|x_p - x_q\|^2) \quad (7)$$

where $\|\cdot\|$ is the Euclidean distance, σ is the kernel width, and γ is the kernel parameter.

4) *CNN*: It is a DL method that has been widely used for feature learning on images. A CNN has a cascade connection

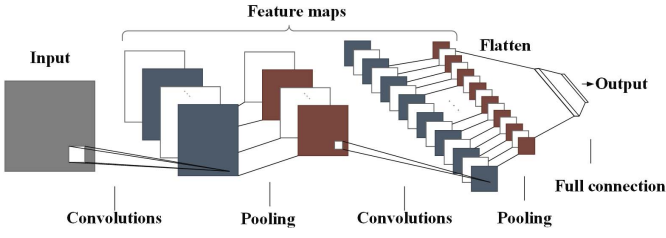


Fig. 2. Structure of the CNN.

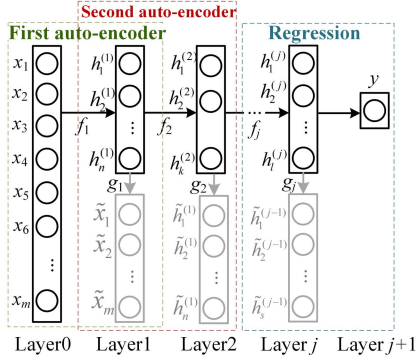


Fig. 3. Structure of the SAE.

structure, as exemplified in Fig. 2 [39], including an input layer, a series of convolution layers, pooling layers, and fully connected layers. The convolutional layer uses the convolutional operation, in which kernels slide over the signals with a stride s to achieve weight sharing. Let $X_i \in R^{h \times w}$ be the 2-D input maps (receptive field) and $K_j \in R^{k_1 \times k_2}$ be the kernels. The convolution operation is expressed as (8), where b_j denotes the bias and \otimes is the discrete convolution operator

$$Y_j = \sum X_i \otimes K_j + b_j. \quad (8)$$

The output of the convolution Y_j is known as the feature map and the original input size $h \times w$ is updated as $\tilde{h} \times \tilde{w}$

$$\begin{cases} \tilde{h} = \frac{h + 2p - k_1}{s} + 1 \\ \tilde{w} = \frac{w + 2p - k_2}{s} + 1 \end{cases} \quad (9)$$

where p is the zero-padding parameter added to the input.

Pooling reduces the dimension of the outputs from the convolutional layer and prevents overfitting. At full connection layers, the neurons are fully connected to all the activations in the previous layers as a standard neural network.

5) SAE: It is constructed by multiple layers of autoencoders, in which the neural networks are trained by performing encoding and decoding.

A typical SAE is illustrated in Fig. 3, and the training process is that the input x is transformed to the hidden layer $h^{(1)}$ by adopting an encoding function f_1 and then the decoding function g_1 reconstructs the original input from the hidden representation as a result of obtaining the first-order characterization of the input data. After that, keep the parameters of the network intact and use these characteristics as input to train the parameters of the second hidden layer $h^{(2)}$.

For feature learning, the reconstruction loss functions of each autoencoder are expressed as

$$L_1(X, \tilde{X}) = \sum_{J=1}^m (x_J - g_1(f_1(\tilde{x}_J)))^2 \quad (10)$$

$$L_2(H^{(1)}, \tilde{H}^{(1)}) = \sum_{J=1}^n (h_J^{(1)} - g_1(f_1(\tilde{h}_J^{(1)})))^2 \quad (11)$$

where L_1 is the loss function with regard to the training samples $X = x_1, x_2, \dots, x_m$ and $\tilde{X} = \tilde{x}_1, \tilde{x}_2, \dots, \tilde{x}_m$ as the reconstructed inputs. L_2 is the loss function of the second autoencoders. $H^{(1)} = h_1^{(1)}, h_2^{(1)}, \dots, h_n^{(1)}$ are the hidden variables of the first autoencoder and $\tilde{H}^{(1)} = \tilde{h}_1^{(1)}, \tilde{h}_2^{(1)}, \dots, \tilde{h}_n^{(1)}$ are the reconstructed hidden variables obtained by the second autoencoder.

6) DBN: Different from the SAE, DBN is stacked by several restricted Boltzmann machines (RBMs), where each hidden layer serves as a visible layer for the next subnetwork and a linear regression is used at the top of the stack [40]. An RBM is a generative stochastic ANN with no direct weighted connection between the visible variables $X = \{x_1, x_2, \dots\}$ and the hidden variables $H = \{h_1, h_2, \dots\}$, aiming to learn a probability distribution over inputs. With this motivation, the joint probability distributions over the visible and hidden neurons $P(x, h)$ are first defined based on a Gaussian energy function $E(x, h; \theta)$, where $\theta = \{w, b, a\}$ is the parameter set of an RBM. Equations (12) and (13) provide the calculation of $P(x, h)$ and E

$$P(x, h; \theta) = \frac{e^{-E(x, h; \theta)}}{\sum_{x, h} e^{-E(x, h; \theta)}} \quad (12)$$

$$E(x, h; \theta) = \sum_{i \in \text{visible}} \frac{(a_i - x_i)^2}{2\sigma_i^2} + \sum_{j \in \text{hidden}} \frac{(b_j - h_j)^2}{2\sigma_j^2} - \sum_{i, j} \frac{x_i h_j}{\sigma_i \sigma_j} w_{ij} \quad (13)$$

where σ_i and σ_j are the standard deviations of Gaussian noise of the visible unit i and the hidden unit j , respectively, and in the iteration, an RBM uses the conditional probability $P(h|x)$ to acquire the state of the hidden unit h_j , while uses $P(x|h)$ to calculate the state of the visible layer x_i . The conditional probability is given as

$$P(h = 1|x; \theta) = \delta \left(\sum_{i \in \text{visible}} w_{ij} x_i + b_j \right) \quad (14)$$

$$P(x = 1|h; \theta) = \delta \left(\sum_{j \in \text{hidden}} w_{ij} h_j + a_i \right). \quad (15)$$

Then, the whole RBM is trained by maximizing the following likelihood function by applying the stochastic gradient ascent algorithm, where X is the set of input variables. Fig. 4 illustrates an exemplary DBN with two RBMs and one perceptron for regression

$$\ln L_{\theta, X} = \sum_{x \in X} P(x, \theta). \quad (16)$$

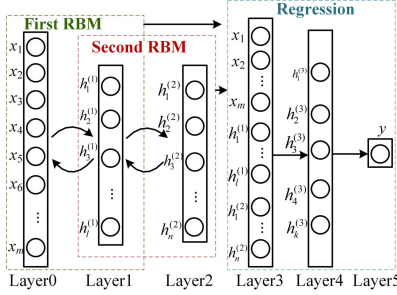


Fig. 4. Structure of the DBN.

D. Performance Evaluation

To evaluate the overall performance of the ML-based energy modeling techniques, a tenfold cross-validation approach is adopted. First, the samples are randomly divided into ten disjoint portions, one of which is used to verify the performance of the techniques, while the rest is regarded as the training set. Then, the same process is repeated ten times by shifting the training and the testing set. At each turn, five performance metrics as defined below are calculated and the final values are their respective mean values from ten evaluations.

1) Mean Absolute Forecasting Error (MAE):

$$\text{MAE}(X, h) = \frac{1}{m} \sum_{i=1}^m |h(x^{(i)}) - y^{(i)}| \quad (17)$$

where m is the number of testing instances, and $y^{(i)}$ and $h(x^{(i)})$ represent the i th observed and predicted values, respectively.

2) Root-Mean-Square Error (RMSE):

$$\text{RMSE}(X, h) = \sqrt{\frac{1}{m} \sum_{i=1}^m (h(x^{(i)}) - y^{(i)})^2}. \quad (18)$$

3) Average of Absolute Error (MAPE):

$$\text{MAPE}(X, h) = \frac{1}{m} \sum_{i=1}^m \frac{|h(x^{(i)}) - y^{(i)}|}{y^{(i)}}. \quad (19)$$

4) Coefficient of Variation of Root-Mean-Square Deviation (CV-RMSE):

$$\text{CV-RMSE}(X, h) = \sqrt{\frac{m \sum_{i=1}^m (h(x^{(i)}) - y^{(i)})^2 / \sum_{i=1}^m y^{(i)}}{m}}. \quad (20)$$

5) Coefficient of Determination (R^2): The mean value for the coefficient of determination (R^2) from the evaluations is shown in (21) at the bottom of the page.

Among them, MAE, RMSE, and MAPE are used to measure the deviation between the actual energy consumption and the prediction energy consumption. The lower MAE, RMSE, and MAPE present better prediction performance of the models.

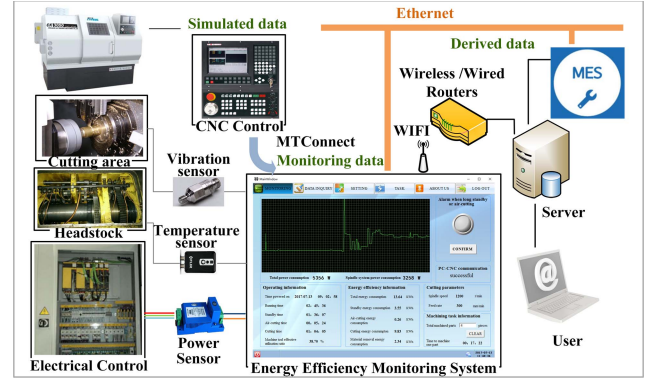


Fig. 5. Hardware platform and information flow in data acquisition platform.

CV-RMSE is defined as the RMSE normalized to the mean of the observed values. Always, we wish our model with lower CV-RMSE. R^2 indicates the extent to which the energy is predictable. In common, the higher the R^2 , the better the prediction model fits the observations.

IV. EXPERIMENTAL SETUP

A. Data Collection

The raw data collected for energy modeling can be classified into three types as follows.

- 1) Simulated data cover the data collected from an ISO 6983 program, which mainly includes “cutting strategy,” “tool type,” “trajectory,” and “machining parameters.” Simulated data govern the practical machining, and it is always regarded as reliable and relatively error-free.
- 2) Monitoring data are generated at the sensor level, representing the observation and measurement of “machine state,” “instantaneous power,” “tool wear,” and “motor temperature.” Monitoring data are collected by the measurement devices. Although the accuracy and precision of these devices are getting higher, noisy or missing data are inevitable, which adversely affect the prediction performance of energy models.
- 3) Derived data, such as “operation,” “machine,” “tool,” “workpiece,” and “cooling,” are referred to as the information that is stored in the existing production management system, e.g., manufacturing execution system (MES). Obviously, errors presented in MES might propagate to the derived data.

As shown in Fig. 5, a data acquisition platform is built through Internet of Things (IoT) and sensing techniques to capture continuously the monitoring data, simulated data, and derived data. Three different types of monitoring data are acquired, including the power signals measured by a power sensor installed in an electrical cabinet, the temperature signals through thermal imaging installed in the headstock, and the vibration signals through a multichannel vibration sensor.

$$R^2(X, h) = \frac{(m \sum_{i=1}^m y^{(i)} h(x^{(i)}) - \sum_{i=1}^m h(x^{(i)}) \sum_{i=1}^m y^{(i)})^2}{(m \sum_{i=1}^m (h(x^{(i)})^2 - (\sum_{i=1}^m h(x^{(i)})^2) \cdot (m \sum_{i=1}^m (y^{(i)})^2 - (\sum_{i=1}^m y^{(i)})^2))}. \quad (21)$$

installed in the cutting area. The total power, spindle power, temperature, and vibration are transmitted to an industrial personal computer, where an energy efficiency monitoring system (EEMS) is used as the interface to process the data for calculating the energy components and acquiring energy efficiency in real time [34]. EEMS accesses the simulated data from the computer numerical control (CNC) system through MTConnect [22]. MES is used as the interface for acquiring the derived data. With the Ethernet based on the transmission control protocol/Internet protocol (TCP/IP), the obtained information is transmitted to an application server through a wireless router. Then, all the information that needs to be preprocessed is then well prepared.

B. Data Preprocessing

Data preprocessing is essential for any ML-based modeling approach, which may include data cleaning, data transformation, and data reduction. Data cleaning is the process of detecting and correcting the missing, incorrect, or noisy parts of the raw data. Ready-made software tools such as DataWrangler and FineBI make it possible for technologists to conduct data cleaning in a quick and easy way. Data transformation includes normalization, smoothing, and aggregation of the raw data. The data covered in this article can be divided into four groups: continuous data, discrete data, image data, and time series data. The following gives the data transformation methods for each type of data in detail.

1) *Continuous Numeric Data*: They refer to the data measured on a continuous scale. The variables $\{x_1, x_2, x_3, x_5, x_6, x_8, x_9, x_{10}\}$ in our case fall into this category. Z-score standardization is adopted to eliminate the influence of dimension. After converted by (22), the data are subject to normal distribution

$$x' = \frac{x_i - \bar{x}}{\sqrt{\frac{1}{N} \sum_{i=1}^N (x_i - \bar{x})^2}} \quad (22)$$

where x' is the standardized variable, x_i is the i th data, \bar{x} is the mean value, and N is the number of data.

2) *Discrete Numeric Data*: They refer to the data that are qualitatively or categorically labeled. The variables $\{x_4, x_7, x_{11}, x_{12}, x_{13}\}$ in our case belong to this category. Specifically, $x_4(m_t) = \{\text{"C2-360HK," "C2-50HK," "CHK460," "CHK560"}\}$, $x_7(t_m) = \{\text{"High-speed steel," "Cemented carbide," "Cermets"}, x_{11}(w_m) = \{\text{"A36," "B211," "A266-I," "No45B," "S41000," "6470E," "A266-III," "A335-P5," "5140," "A306GR55"}\}$, $x_{12}(w_h) = \{\text{"Annealing," "Normalizing," "Quenching," "Tempering"}\}$, and $x_{13}(c_o) = \{\text{"Dry cutting," "Wet cutting"}\}$. In order to represent them numerically, the one-hot encoding method is adopted to convert the qualitative variables into quantitative ones. This approach uses a vector of N binary bits to replace a qualitative value with N possible, where only a single bit is nonzero to indicate the corresponding category. This is to say when the original feature evaluates to the i th qualitative value, the i th extended feature equals to 1 and others set as 0. For instance, m_t is coded as $x_4 = \{(1000) = \text{'C2-360HK'}, (0100) = \text{'C2-50HK'}, (0010) = \text{'CHK460'}, (0001) = \text{'CHK560'}\}$.

TABLE I
DATA SET USED IN THE COMPARATIVE STUDY

Dataset	Features	Collection time	Data size
D1	$\{x_1, x_2, \dots, x_{13}\}$	2016.10.12-2016.11.25	1500 instances
D2	$\{x_1, x_2, \dots, x_{13}\}$	2017.10.12-2017.12.4	1500 instances
D3	$\{x_1, x_2, \dots, x_{13}\}$	2018.10.12-2018.11.24	1500 instances
D4	$\{x_1, \dots, x_{14}, x_{15}\}$	2017.3.12-2017.8.21	5 months
D5	$\{x_1, \dots, x_{14}, x_{15}\}$	2018.10.12-2019.3.16	5 months

3) *Image Data*: They are represented as a pixel matrix. The temperature field for a target spindle motor is continuously collected through thermal imaging with the interval of 2 s. The data $x_{14}(m_o)$ in the form of a 96×96 gray-scale input image are recorded when the motor reaches to thermal balance (temperature is relative stable).

4) *Time-Series Data*: They are taken successively at equally spaced points in a temporal order. The vibration signal has a natural temporal ordering, and in the metal cutting process, the increment in tool wear increases the signal magnitude. Thus, vibration signals are recorded to characterize the current tool wear condition $x_{15}(t_w)$. Aimed at the nonstationary property of the vibration signal, the time window method incorporated with short-time Fourier transform (STFT) is adopted to transfer the time-domain data into the frequency domain data. Specifically, the vibration signals are first captured using three-channel vibration sensors installed around the cutting area, and the size of the raw data is $3 \times L \times D$, where L denotes the time window length and D is the number of segments. Then, the raw data are transferred through STFT, based on which the key frequency bands are intercepted according to the variation magnitude of vibration frequency. Finally, the time series of the vibration data can be clipped into $3 \times S \times D$, where S is the truncation length.

Data reduction is used to reduce the dimension of the data set. It is a process to extract the essential information and remove the one that is useless. The commonly used data reduction methods are principal component analysis (PCA) that transforms the multivariate data set from its raw inside-correlated form to the uncorrelated one [41], ReliefF algorithm that exams the feature difference between the nearby samples and determines the final features via iteratively calculating the feature weights [42], and fuzzy C-means that calculates the similarity degree of the input samples [43]. Through removing the nondiscriminative features, the computational efficiency and prediction performance of the ML algorithms may be enhanced.

C. Data Set Description

For this study, five data sets (see Table I) are collected over the course of three years and used for two different cases in evaluating the performance of the considered models. Deterioration of the tool and the spindle motor is not considered in the data sets D1–D3. These data sets collected one year apart are used separately and/or in combination for Case 1 to analyze the variation of model errors. It helps us to judge whether the input variables are sufficient for energy efficiency modeling by observing the variation of prediction accuracy with the increase in the amount of training data. Features including tool wear and spindle motor aging are involved in Case 2.

By training the models on data sets D4 and D5, the necessity and benefits of introducing these two features are investigated.

V. RESULTS AND DISCUSSION

A. Case 1 (Modeling the Energy Efficiency Without Considering Tool Wear and Spindle Motor Aging)

It can be widely observed in literature [18]–[23] that energy models were always established without considering tool wear and spindle motor aging due to the stringent controls on processes and resources under laboratory environments. Thus, in Case 1, we test whether the ML algorithms can achieve the expected performance when these two dynamic features are ignored in energy efficiency modeling for practical applications.

1) *Model Description:* Considering that the training data in Case 1 are small in feature dimension (no more than 31 features) and data quantity (no more than 5000 instances), only traditional ML methods, i.e., ANN, SVR, and GPR, are used to train the energy efficiency models. The input vectors and the corresponding energy efficiency are directly fed into the three models so as to reveal the best performance methods. All the ML methods have several hyperparameters that should be tuned according to the data set to achieve optimum prediction performance, and the details are given as follows.

In the case of ANN models, four hyperparameters {momentum, learning rate, transfer function, and batch size} are tuned. The momentum helps to accelerate the convergence. The learning rate controls how fast the neural network learns in the training period. The transfer function is used to increase the nonlinear characteristics. The batch size is to regulate the generalization ability. The mean-square error (MSE) between the target value and the predicted value is adopted as the loss index for ANN training. The iteration number is decided in corresponding to the gap between underfitting and overfitting. For our case, 500 is chosen for the reason that the gap between the training and testing errors is the smallest. The ANN architecture in Case 1 is finally determined as 31-128-64-1.

The hyperparameters {kernel type, kernel parameter γ , regularization constant C , and epsilon ε } of the SVR models are quiet important. The kernel type is set to “RBF,” considering its strong anti-interference ability of the system with observation noise. γ is to control the generalization ability of the algorithm. C is related to the complexity and stability of the algorithm. ε regulates the error. In the training process, the weight and bias values are updated according to the scaled conjugated gradient method. The stopping criterion is set to $1e-3$. Optimal hyperparameter settings can be determined by intelligent optimization methods [44]–[46], Bayesian optimization [47], trial-and-error [48], and so on. Among these methods, trial-and-error is chosen for acquiring the hyperparameters of ANN and SVR in this article, considering its simplicity, effectiveness, and cost savings.

In contrast to ANN and SVR, the hyperparameters of the GPR models, as given by (5), are inferred by using the empirical Bayes approach for the given training data sets. The length-scale parameter of the kernel function is initialized as $\ell = 1$. The interval ranges of standard deviation are

TABLE II
MODEL PARAMETERS USED IN CASE 1

Method	Hyper-parameters	D1/D2/D3	D1+D2	D1+D2+D3
SVR	Kernel parameter	0.25	0.28	0.30
	Regularization constant	1e+4	1e+4	1.2e+4
	Epsilon	0.28	0.26	0.35
ANN	Alpha(momentum)	0.48	0.35	0.35
	Learning rate	1e-3	2e-4	2e-4
	Transfer function	‘ReLU’	‘ReLU’	‘ReLU’
GPR	Batch size	34	68	68
	Length scale parameter	0.364	0.359	0.350
	Vertical scale parameter	0.088	0.052	0.051
	Noise variance	0.00026	0.00038	0.00043

set to $\mu \in [0.01, 0.1]$ and $\vartheta \in [0.0001, 0.001]$. We adopt the method presented in [31], where the grid search method and tenfold cross-validation are performed to acquire the optimal parameters. The determined hyperparameters are also presented in Table II.

2) *Model Analytical Results:* Table III reports the mean value and its standard deviation (mean std) of MAE, MAPE, RMSE, and CV-RMSE for the above methods in ten simulations to compare the accuracy and stability. The values in bold indicate the performance metrics that are the best among the various prediction models. In general, errors on the testing data set suggest the generalization ability of the developed models, while errors on the training data set suggest the goodness-of-fit. The energy efficiency models in Scenarios 1–3 are trained on D1–D3 with the same amount of data, respectively. It can be found clearly that as for the training data set, SVR has the best MAE and MAPE in Scenario 1, and the best MAE in Scenario 2. Notably, GPR performs consistently better than the other two algorithms in terms of all metrics on the testing data set, indicating the strong nonlinear mapping generalization ability and good fitting performance of GPR.

Standard deviation reveals the stability of the model. From the standard deviation values, GPR is the most stable algorithm for establishing energy efficiency models followed by SVR and ANN. Even though the models are acceptable from the industrial point of view, the prediction accuracy is limited (R^2 value only up to 0.935) in contrast to the high accuracy provided in [18], where R^2 reached to 0.999. We surmise the reasons from two aspects. The first is about the data. It can be widely found in literature [18]–[23] that models were always established with stringent controls on processes and resources under laboratory environments. Instead, our models are established with the data from real practice, where the operations and machining configurations are more interactive and dynamic, and thus, the energy data may be mixed up with a loud and neglected noise. Second, some significant features are missed into the models.

Models are trained on a combination of D1 and D2 in Scenario 4 and a combination of D1–D3 in Scenario 5. Simulation results in Scenario 4 show that the mean values of MAE and MAPE for the ANN are at the minimum points; the standard deviations are too large compared with GPR that has the second-smallest mean value and the lowest standard deviation. From the statistical RMSE, CV-RMSE, and R^2 , the prediction performance of the GPR models is superior

TABLE III
COMPARATIVE MODELS OF SVR, GPR, AND ANN ON DIFFERENT DATA SETS

Scenario 1 (Dataset:D1)											
Method	Training						Testing				
	MAE	RMSE	MAPE	CV-RMSE	R ²	MAE	RMSE	MAPE	CV-RMSE	R ²	
ANN	79.70±1.32	115.4±1.83	11.06±0.31	0.134±0.0021	0.942	89.07±6.43	126.6±14.5	12.39±0.85	0.147±0.0116	0.929	
GPR	75.32±0.78	109.1±1.47	10.44±0.08	0.127±0.0013	0.949	84.70±7.22	121.8±15.7	11.91±0.56	0.141±0.0136	0.934	
SVR	72.29±0.67	113.5±1.51	10.10±0.14	0.132±0.0013	0.944	84.86±7.20	123.6±16.8	12.02±0.64	0.143±0.0145	0.933	
Scenario 2 (Dataset:D2)											
Method	Training						Testing				
	MAE	RMSE	MAPE	CV-RMSE	R ²	MAE	RMSE	MAPE	CV-RMSE	R ²	
ANN	90.66±1.91	142.7±2.64	12.76±0.28	0.166±0.0030	0.922	95.32±12.36	146.0±18.3	13.46±1.71	0.169±0.0305	0.916	
GPR	90.85±1.26	135.1±2.36	12.61±0.18	0.157±0.0025	0.931	95.05±10.53	141.5±17.5	13.36±1.61	0.165±0.0186	0.921	
SVR	90.57±1.07	142.3±2.49	12.77±0.24	0.166±0.0024	0.923	96.86±10.59	146.0±18.4	13.69±1.47	0.169±0.0203	0.915	
Scenario 3 (Dataset:D3)											
Method	Training						Testing				
	MAE	RMSE	MAPE	CV-RMSE	R ²	MAE	RMSE	MAPE	CV-RMSE	R ²	
ANN	96.19±1.46	135.4±2.36	13.51±0.27	0.157±0.0027	0.930	101.32±10.73	143.0±17.5	14.18±1.61	0.167±0.0196	0.920	
GPR	82.99±0.98	130.2±2.37	11.51±0.18	0.151±0.0025	0.937	90.03±9.24	135.3±13.3	12.52±1.38	0.157±0.0157	0.929	
SVR	95.85±1.42	135.1±2.30	13.61±0.27	0.157±0.0024	0.932	100.95±10.53	141.5±16.1	14.36±1.39	0.165±0.0204	0.921	
Scenario 4 (Dataset: D1+D2)											
Method	Training						Testing				
	MAE	RMSE	MAPE	CV-RMSE	R ²	MAE	RMSE	MAPE	CV-RMSE	R ²	
ANN	109.99±2.35	174.2±2.75	15.00±0.23	0.203±0.0023	0.869	113.64±9.16	175.9±24.0	15.51±1.93	0.205±0.0242	0.864	
GPR	109.89±0.99	157.4±2.88	15.55±0.26	0.183±0.0040	0.891	115.24±8.01	163.9±22.2	16.24±1.34	0.191±0.0227	0.882	
SVR	113.55±1.32	165.9±2.29	16.01±0.27	0.190±0.0028	0.887	116.09±8.72	167.8±23.9	16.45±1.52	0.196±0.0283	0.872	
Scenario 5 (Dataset: D1+D2+D3)											
Method	Training						Testing				
	MAE	RMSE	MAPE	CV-RMSE	R ²	MAE	RMSE	MAPE	CV-RMSE	R ²	
ANN	120.42±1.49	189.8±3.70	15.98±0.19	0.221±0.0038	0.844	124.34±17.03	189.9±35.34	16.56±1.91	0.220±0.0379	0.842	
GPR	117.03±1.42	184.8±3.47	15.66±0.20	0.215±0.0038	0.852	121.33±15.65	185.5±24.93	16.28±0.67	0.215±0.0375	0.849	
SVR	119.52±1.43	183.1±3.42	15.29±0.13	0.215±0.0036	0.851	121.33±16.91	186.8±37.21	16.77±1.82	0.214±0.0213	0.849	

to that of the ANN and SVR models. The comparisons in Scenario 5 show that SVR has the best performance on CV-RMSE but GPR succeeds to find better values in terms of other four performance metrics. The standard deviation values of SVR are slightly better than that of ANN, while GPR outperforms SVR and ANN from both accuracy and stability. It is worth mentioning that the amount of data in Scenarios 4 and 5 are twice and three times as much as that in Scenarios 1–3. However, the model accuracy of all the mentioned algorithms drops congruously with an increase in the spread of the data collection time. This effect may be significant when using the models established three years ago to predict the energy efficiency in the current situation. In our case, the GPR model error increases by 7.2%, which may be rejected in practice.

3) *Analysis of Training Data Set Size and Training Time:* In this section, we further discuss the behavior of the ML models in terms of the number of training samples and training time. The training data set size mainly corresponds to the training efficiency and prediction accuracy of the models. Fig. 6(a)–(c) depicts the learning curves to figure out the effect of the training data set size on models' predictive performance. We use R² score function to validate the models, based on which the learning curves are drawn to show the training and testing scores of the models for varying numbers of training samples. Three data sets with different data capacities are investigated. It can be seen from the figures that when the amount of training data is small, testing scores are much lower than the training scores. This means that training with a

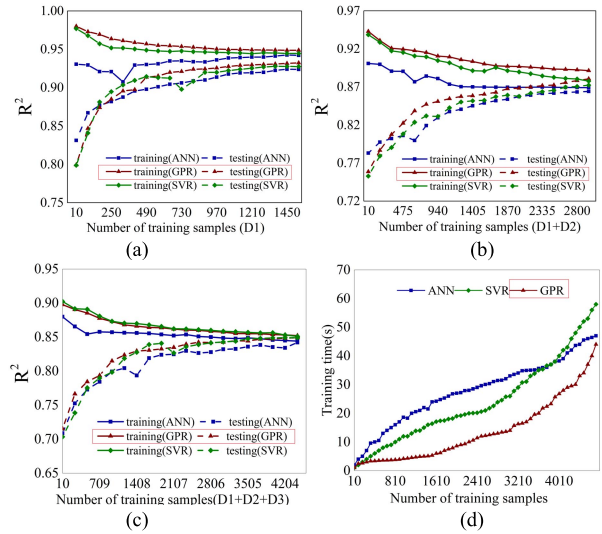


Fig. 6. Effects of the number of training samples on (a)–(c) prediction accuracy and (d) training time.

small data set can cause the estimator to memorize all training examples, in turn leading to poor performance on a testing data set. In this way, increasing the training data would increase the model generalization (i.e., the prediction capacity of the unseen testing data set). However, since more data noise and uncertainties exist in the training set, the training scores keep descending. Note that there are some inflection points in the learning curves. For instance, in Fig. 6(a), the accuracy of the ANN model on the training data set keeps dropping until

the sample number increases to 330. This result is due to the instability of the algorithms and the usage of hyperparameters independent of the data set. Even though it is helpful to analyze the fitting performance, it can be seen that GPR shows best performance on both training and testing data sets, while the ANN shows the relatively lower accuracy than GPR and SVR. However, the best convergence scores are no more than 0.935 for the testing set and 0.949 for the training set with the increase in the number of training samples, indicating the underfitting of the constructed GPR models. At this point, high prediction errors are intensified by the insufficient feature used in the models and we will not benefit much from adding more training data.

Training time is mainly affected by the model complexity, feature selection, and number of training data. In a similar fashion of learning curve, Fig. 6(d) is depicted to investigate the effect of training data size on training time for different algorithms. As for the ANN models, training time is almost linear with sample number and ANN is the most time-consuming algorithm, whereas SVR has a higher training time when the training sample grows to 3700. The training time of SVR and GPR is more sensitive to the training data size and the time increases exponentially especially when the number of training samples is larger than 2410. GPR shows a consistent lower training time than SVR and ANN. Therefore, GPR is strongly recommended to build the energy efficiency model in this case considering its high efficiency and good fitting performance.

B. Case 2 (Energy Efficiency Modeling Considering Deterioration of Spindle Motor and Cutting Tool)

The evaluation results in Case 1 show that training the models with 13 static features cannot meet the needs of high-precise prediction of energy efficiency. Thus, in Case 2, signals of spindle motor temperature and cutting area vibration, which represent motor aging and tool wear conditions, are added into the models so as to test whether dynamic features improve prediction performance.

1) Architectures of DL Networks: Three typical DL models including CNN, SAE, and DBN are designed for the image and time series processing tasks. After looking at the required input and output format, the design of deep network architectures used in our study is described as follows.

a) Network input: The networks receive two kinds of signals as their input. The gray-scale temperature signals are with 96 pixels wide and 96 pixels high. As for the three-channel vibration signals, set $L = 1000$, $D = 250$, and $S = 250$. To use 2-D convolution operation, we match the input size from the original $3 \times 250 \times 250$ by three channels $\times (250 \times 250)$ pixels). The SAE and DBN use the same temperature and vibration signals that are flattened as 9216 and 187500, respectively.

b) Feature extraction: The CNN consists of several convolutional layers with 2-D convolutions. For instance, the input temperature signals are convolved by 16 filters with a kernel of dimension 3×3 . Each convolution is followed by ReLU activation function and a max-pooling layer. The overall CNN architecture for feature extraction is shown in Fig. 7. Different

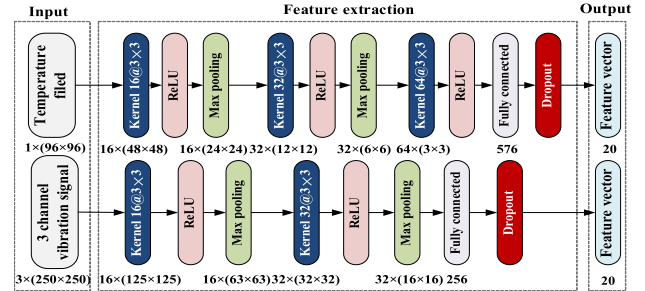


Fig. 7. Graphical representation of the CNN structure implemented in Case 2.

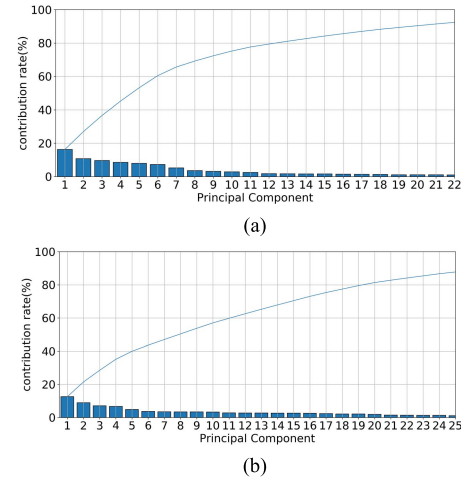


Fig. 8. Data reduction of (a) temperature data and (b) vibration data using PCA.

from CNN, SAE and DBN need to pretrain the SAE and RBM. As a performance comparison, the architecture of SAE for temperature signals is set as 9216-4608-2300-1285-20, while that of DBN is set as 9216-4369-2000-1250-20. In a similar way, we use the SAE of architecture 187500-56835-1925-328-20 to extract the features for the vibration architecture. The DBN architecture is 187500-49245-3532-573-20.

c) Regression: To fit the energy efficiency, we use a fully connected layer followed by standard dropout regularization for reducing overfitting. After that, the features are deduced to ten units. Based on the backpropagation (BP) with a batch size of 16, the CNN is then trained by the minimization of the MSE loss function. For SAE and DBN, weights of all hidden layers are initialized through unsupervised learning at the pretraining period. Then, fine-tuning of the entire SAE and DBN is employed using the labeled samples. All the weights are updated by the gradient descent strategy with the Adam optimizer algorithm.

During the network training process, the network structures and the parameters shown in Table IV are determined by trial and error, with the result shown in Table V. It is worth mentioning that to reduce the computational overhead and improve the performance of SVM, ANN, and GPR, PCA is used to remove the nondiscriminative features. With the eigenvalue decomposition (EVD) of a matrix, a set of observations of the original temperature and vibration features can be converted into a set of values of linearly uncorrelated variables called principal components. Variance explained of each principal is regarded as the contribution rate (see Fig. 8). After the feature

TABLE IV
MODEL PARAMETERS USED IN CASE 2

Method	Hyper-parameter	D4/D5	D4+D5
SVR	Kernel parameter	0.33	0.35
	Regularization constant	1.5e+4	1.7e+4
	Epsilon	0.15	0.15
ANN	Alpha(momentum)	0.04	0.04
	Learning rate	1e-3	1.5e-3
	Transfer function	'ReLU'	'ReLU'
GPR	Length scale parameter	0.293	0.282
	Vertical scale parameter	0.0341	0.0332
	Noise variance	0.00076	0.00079
CNN	Learning rate	1e-4	9e-3
	Weight decay (L2 penalty)	1e-5	1.6e-5
	Stride	2	2
SAE	Padding	1	1
	Dropout probability	1e-3	9e-3
	Pre-training times	750	1000
DBN	Fine-tuning times	1000	1500
	Learning rate in pre-training	1.5e-4	1.6e-4
	Learning rate in fine-tuning	1e-4	1e-4
DBN	Weight decay (L2 penalty)	1e-5	5e-5
	Activation function	'Sigmoid'	'Sigmoid'
	Dropout	1e-3	2.5e-3
DBN	Pre-training times	1000	1750
	Fine-tuning times	3000	4500
	Learning rate in pre-training	1e-5	1.75e-5
DBN	Learning rate in fine-tuning	1e-5	2e-5
	Weight decay (L2 penalty)	1e-5	1e-5

dimension reduction, temperature/vibration feature would be used and combined with other 31 variables for energy modeling, so equalization of variables should be also considered. To that end, temperature and vibration features are reduced to 22 and 25 principal components with accumulated contribution rates of 87.48% and 85.63%, respectively.

2) *Model Comparison*: In this section, we compare three traditional ML models and three DL models. It is obvious from the results provided in Table V that all the DL models take absolutely dominant positions on MAE, MAPE, RMSE, CV-RMSE, and R^2 over the traditional ML models, indicating that DL models can capture the features of temperature data and the characteristics of the vibration data series, achieving better energy efficiency prediction performance. Among the mentioned traditional ML algorithms, GPR models are found dominant in relative accuracy with an R^2 increase of 0.5%–1.1% as compared favorably with SVR and ANN. It is seen that in all scenarios, the results of the CNN are generally better than MAE, MAPE, and R^2 , while only the mean RMSE in Scenario 8 is 4.84% higher than the minimum point produced by SAE and the similar result can be found in Scenario 6 where the mean CV-RMSE of the CNN is 1.28% higher than that of SAE. On the contrary, SAE shows relatively lower prediction accuracy than the CNN, but the standard deviations are almost all at minimum points, which indicates that SAE models are the most stable. DBN is mediocre among the three DL methods either in prediction or in stability performance. Still, it possesses a high accuracy, whose R^2 can be increased by 2.9% at most compared with the traditional ML models.

The simulations of different algorithms on D4 and D5 reveal that introducing vibration data improves the accuracy of energy efficiency prediction. However, the improvement in the

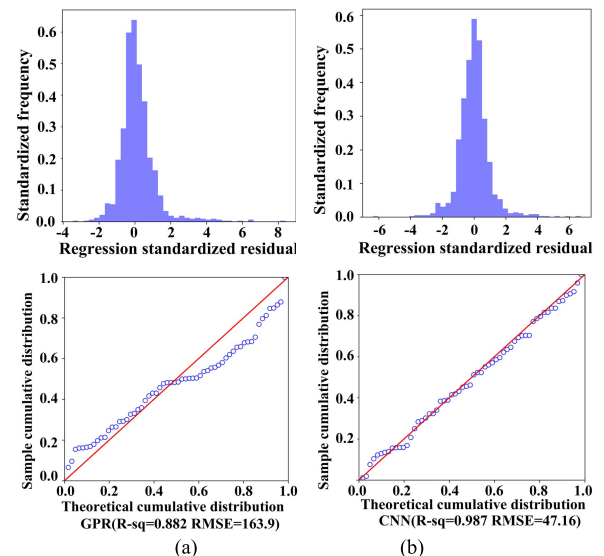


Fig. 9. Frequency distribution and P-P plots of measured and simulated energy efficiency.

traditional ML models is not much obvious. The undesirable errors are mostly likely to derive from feature extraction by PCA, leading to the loss of available information. Thus, it can be stated that DL outperforms traditional ML in terms of image and time-series applications. Models are also trained on a reconstructed data set with a fusion of D4 and D5. Since the interval of collection time is seven months, this simulation reflects the error source from the temporal aspect.

Residual analysis is conducted for the GRP model in Scenario 4 and the CNN model in Scenario 8. The difference mainly comes from whether tool wear and spindle motor aging are considered or not; 60 testing points are randomly selected to assess the goodness of fit of these two models. It follows from Fig. 9 that the frequency values are almost normal distribution. However, the data of GPR are skewed left and show a kurtosis, which confirms the poor performance of the developed GPR model. Likewise, P-P plot (probability–probability plot) is used to evaluate how closely the measured and appointed data sets agree. It is seen that all validation data of the CNN are close to the bisector line, demonstrating that the proposed CNN model can be applied in high reliability. Comparing the results with the CNN, we deduce that a majority of the errors derived from a reaction to the tool wear and spindle motor aging condition change, for which the GPR model has not been trained. The models ignoring spindle motor aging only work within a short period of time, and they require a periodic update to ensure the prediction accuracy. In addition, the error caused by tool wear persists due to the fact that the cutting tools under different wear conditions are promiscuously used in the practical machining processes.

Now, we focus on the learning curve analysis of the algorithms. All developed models react in a gradual way to an increase in the training sample size. The plot is given in Fig. 10(a). It can be seen that the training scores of different algorithms converge consistently to high values, and the performance of the testing set is enhanced with the increasing

TABLE V
COMPARATIVE MODELS OF SVR, GPR, ANN, CNN, SAE, AND DBN ON DIFFERENT DATA SETS

Scenario 6 (Dataset:D4)											
Method	Training						Testing				
	MAE	RMSE	MAPE	CV-RMSE	R ²	MAE	RMSE	MAPE	CV-RMSE	R ²	
ANN	74.04±1.57	100.73±1.87	10.61±0.22	0.117±0.0019	0.95582.57±7.0612.73±10.7711.88±1.02	0.137±0.0104	0.939				
GPR	70.48±0.67	96.35±0.90	10.14±0.10	0.112±0.0009	0.95879.24±6.25108.16±9.51	11.57±0.79	0.126±0.0091	0.946			
SVR	67.71±0.60	99.67±1.09	9.82±0.15	0.116±0.0013	0.95680.02±5.8510.77±11.3411.72±0.69	0.129±0.0101	0.944				
CNN	51.34±1.32	63.93±1.20	7.14±0.35	0.073±0.0014	0.98656.90±3.04	67.98±3.88	8.37±0.72	0.079±0.0042	0.979		
SAE	52.01±0.31	62.68±0.31	7.35±0.09	0.074±0.0014	0.98259.09±2.65	72.34±3.20	8.81±0.53	0.078±0.0029	0.975		
DBN	54.43±1.10	67.13±1.23	7.15±0.25	0.078±0.0023	0.96962.31±3.12	77.41±3.61	8.84±0.62	0.090±0.0032	0.966		
Scenario 7 (Dataset:D5)											
Method	Training						Testing				
	MAE	RMSE	MAPE	CV-RMSE	R ²	MAE	RMSE	MAPE	CV-RMSE	R ²	
ANN	67.71±1.51	99.46±1.92	9.81±0.34	0.116±0.0022	0.95680.17±7.13110.5±12.11	11.73±1.25	0.129±0.0112	0.943			
GPR	67.88±0.86	91.50±0.97	10.24±0.36	0.107±0.0012	0.9593.30±4.52	102.8±5.57	11.44±0.87	0.123±0.0099	0.953		
SVR	69.49±1.17	94.01±1.43	10.02±0.10	0.109±0.0018	0.95878.23±6.01	105.7±9.07	13.69±1.47	0.169±0.0203	0.949		
CNN	50.28±1.73	57.17±0.26	7.82±0.31	0.071±0.0021	0.98757.07±4.43	61.65±14.56	8.79±0.85	0.067±0.0066	0.983		
SAE	45.32±0.48	60.12±0.87	8.04±0.12	0.067±0.0015	0.98259.70±4.22	80.87±5.76	8.83±0.46	0.091±0.0016	0.972		
DBN	52.89±0.97	63.54±1.43	7.88±0.28	0.062±0.0018	0.96870.76±4.20	63.6±6.86	9.62±0.54	0.098±0.0045	0.959		
Scenario 8 (Dataset:D4+D5)											
Method	Training						Testing				
	MAE	RMSE	MAPE	CV-RMSE	R ²	MAE	RMSE	MAPE	CV-RMSE	R ²	
ANN	60.03±0.95	81.56±0.63	8.71±0.08	0.095±0.0015	0.97070.97±3.28	91.32±4.51	10.52±0.93	0.106±0.0079	0.961		
GPR	54.29±0.34	67.08±0.46	7.75±0.04	0.078±0.0008	0.97962.01±3.27	77.39±3.97	8.82±0.57	0.090±0.0048	0.972		
SVR	54.62±0.69	67.61±0.85	7.71±0.08	0.079±0.0012	0.97662.56±4.91	78.05±5.96	8.87±0.74	0.091±0.0060	0.971		
CNN	23.19±1.65	35.47±1.43	5.86±0.31	0.044±0.0044	0.99338.77±8.11	47.16±7.56	7.82±1.63	0.053±0.0096	0.987		
SAE	35.32±0.68	49.19±0.67	5.44±0.28	0.037±0.0023	0.98946.85±2.75	44.98±5.79	8.01±0.56	0.061±0.0026	0.978		
DBN	36.29±0.97	53.52±1.51	5.10±0.24	0.052±0.0031	0.98649.07±5.27	53.46±10.82	9.02±0.64	0.067±0.0045	0.976		

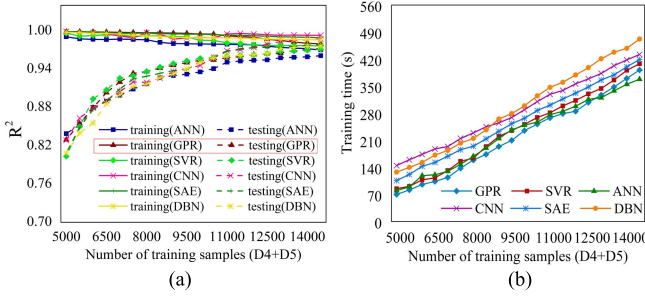


Fig. 10. Effects of the number of training samples on (a) prediction accuracy and (b) training time.

size of the training set. Obviously, the final training scores are a little bit higher than the testing scores. This is due to the concept of overfitting, and thus, models could benefit from more training samples. DL suffers from overfitting problem when the training sample is insufficient due to the complexity of neural networks and large hyperparameters. The conflict is that the increase in more training samples means sacrificing computational time.

Fig. 10(b) depicts the training time consumed in constructing the models in Scenario 8. SVR and ANN have comparable training time on lower number of training samples. However, SVR sustains a great loss in efficiency when the sample number is beyond 10 000. GPR keeps being the most efficient algorithm until the sample number reaches to 13 000. DL is rather time-consuming for model construction. Although the SAE's computing efficiency is satisfactory, it is not able to outperform better than the traditional ML models. DBN has significantly higher training time, as the sample number increases to 7000. Consequently, the use of the DBN models

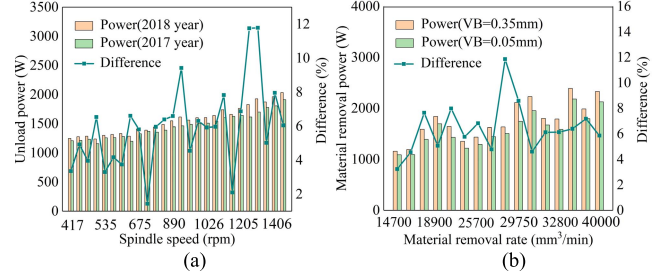


Fig. 11. Effects of (a) spindle motor aging and (b) tool wear on power consumption.

for modeling energy efficiency in the machining system is not suggested due to the highest computing complexity but mediocre performance. It is wise to take a few more seconds to construct CNN models for more accurate prediction, and thus improve the reliability of practical applications.

2) *Effect Analysis of Tool Wear and Spindle Motor Aging:* Additional tests are conducted to further demonstrate the influence of spindle motor aging and tool wear on power consumption. The results are depicted in Fig. 11.

Fig. 11(a) consists of 27 tests performed on the CHK460 CNC lathe. The unload power under the same spindle speed is measured one year after the first records in 2017. The results show a consistent increasing tendency over the whole test, as much as a 10.3% increase can be reached. This can be explained by the aging of spindle motor insulation, which results in a decrease in the electrical insulation resistance, and thereby increase the eddy-current loss associated with the increase in motor temperature and operating current. To assess the impacts of tool wear on power consumption, 16 orthogonal

experiments are conducted under different tool wear conditions [see Fig. 11(b)]. Average width (VB) of the wear land is set as 0.05 and 0.35 mm. Coordinated growth in tool wear and material removal power is observed with an increase up to 11.7%. This is because larger tool wear aggravates the friction between the cutting tool and machined surface of the workpiece, which increases the cutting force. Therefore, we can conclude that the application of temperature and vibration sensors could allow for a more accurate prediction of energy efficiency.

VI. CONCLUSION

This article explores the capabilities of three traditional ML algorithms and three DL algorithms for energy efficiency modeling. Our goal is to find the suitable algorithms in two different scenarios: the first one is modeling under steady-state conditions and the second one considers the effects of spindle motor aging and tool wear on energy efficiency in mechanical machining. The scope of a set of models refers not only the prediction accuracy but also the types of data used, the types of features used, and the sizes of data and computational time. Feature selection and the required data preparation are first reviewed. The performance evaluation is carried out in terms of five reliable and well-known statistical indicators. The sensitivity of ML models to training data size and time is investigated by means of learning curve analysis.

As seen from the comparative study, these two kinds of modeling algorithms have their strengths and weakness. Traditional ML algorithms are more suitable for small sample situations, while DL performance is better with regard to feature learning on images and time series. When spindle motor aging and tool wear are neglected, GPR models perform best in terms of accuracy, stability, and time efficiency. However, underfitting occurs in all the models due to the lack of important feature items and the accuracy cannot be further improved by raising the training data size. Thus, it is necessary to add spindle motor aging and tool wear indexes into the models. DL provides a new viable option for energy efficiency modeling. The simulation results show that CNN, SAE, and DBN have better prediction performance over GPR, ANN, and SVR, whereas the model selection phase is far more complex, which makes it easy for them to come to overfitting.

We are planning to extend our research in the following aspects. An in-depth comparative analysis on additional data sets covering various processes as well as the exploration of additional performance measurements will lead to a comprehensive model comparison. The effort is also aimed at complementing the physics-based models established by prior researchers to improve energy efficiency prediction. The impact and coupling effects of configuration parameters and machining parameters will be further explored.

REFERENCES

- [1] R. S. Altintas, M. Kahya, and H. Ünver, "Modelling and optimization of energy consumption for feature based milling," *Int. J. Adv. Manuf. Technol.*, vol. 86, nos. 9–12, pp. 3345–3363, 2016.
- [2] H. Luoke, T. Renzhong, W. Cai, Y. Feng, and X. Ma, "Optimization of cutting parameters for improving energy efficiency in machining process," *Robot. Comput.-Integr. Manuf.*, vol. 59, pp. 406–416, Oct. 2019.
- [3] J. Tuo, F. Liu, and P. Liu, "Key performance indicators for assessing inherent energy performance of machine tools in industries," *Int. J. Prod. Res.*, vol. 57, no. 6, pp. 1811–1824, 2019.
- [4] S. Ma, Y. Zhang, J. Lv, H. Yang, and J. Wu, "Energy-cyber-physical system enabled management for energy-intensive manufacturing industries," *J. Clean. Prod.*, vol. 226, pp. 892–903, Jul. 2019.
- [5] Z. M. Bi and L. Wang, "Energy modeling of machine tools for optimization of machine setups," *IEEE Trans. Autom. Sci. Eng.*, vol. 9, no. 3, pp. 607–613, Jul. 2012.
- [6] G. Tian, Y. Ren, Y. Feng, M. Zhou, H. Zhang, and J. Tan, "Modeling and planning for dual-objective selective disassembly using AND/OR graph and discrete artificial bee colony," *IEEE Trans. Ind. Informat.*, vol. 15, no. 4, pp. 2456–2468, Apr. 2019.
- [7] G. Tian, M. Zhou, and P. Li, "Disassembly sequence planning considering fuzzy component quality and varying operational cost," *IEEE Trans. Autom. Sci. Eng.*, vol. 15, no. 2, pp. 748–760, Apr. 2018.
- [8] Q. Xiao, C. Li, Y. Tang, L. Li, and L. Li, "A knowledge-driven method of adaptively optimizing process parameters for energy efficient turning," *Energy*, vol. 166, pp. 142–156, Jan. 2019.
- [9] O. V. Arriaza, D.-W. Kim, Y. L. Dong, and M. A. Suhaimi, "Trade-off analysis between machining time and energy consumption in impeller NC machining," *Robot. Comput.-Integr. Manuf.*, vol. 43, pp. 164–170, Feb. 2017.
- [10] H. Liu, E. Miao, X. Zhuang, and X. Wei, "Robust modeling method for thermal error of CNC machine tools based on ridge regression algorithm," *Precis. Eng.*, vol. 51, pp. 169–175, Feb. 2018.
- [11] S. Zeng, X. Wan, W. Li, Z. Yin, and Y. Xiong, "A novel approach to fixture design on suppressing machining vibration of flexible workpiece," *Int. J. Mach. Tools Manuf.*, vol. 58, pp. 29–43, Jul. 2012.
- [12] Q. Xiao, C. Li, Y. Tang, and L. Li, "Meta-reinforcement learning of machining parameters for energy-efficient process control of flexible turning operations," *IEEE Trans. Autom. Sci. Eng.*, to be published, doi: 109/TASE.2019.2924444.
- [13] L. Wu, H. Zhou, X. Ma, J. Fan, and F. Zhang, "Daily reference evapotranspiration prediction based on hybridized extreme learning machine model with bio-inspired optimization algorithms: Application in contrasting climates of China," *J. Hydrol.*, vol. 577, Oct. 2019, Art. no. 123960.
- [14] A. M. Abdulshahed, P. L. Andrew, S. Fletcher, and A. Potdar, "Thermal error modelling of a gantry-type 5-axis machine tool using a grey neural network model," *J. Manuf. Syst.*, vol. 41, pp. 130–142, Oct. 2016.
- [15] N. Zhang and D. Shetty, "An effective LS-SVM-based approach for surface roughness prediction in machined surfaces," *Neurocomputing*, vol. 198, pp. 35–39, Jul. 2016.
- [16] D. Kong, Y. Chen, and N. Li, "Gaussian process regression for tool wear prediction," *Mech. Syst. Signal Process.*, vol. 104, pp. 556–574, May 2018.
- [17] I. Oleaga, C. Pardo, J. J. Zulaika, and A. Bustillo, "A machine-learning based solution for chatter prediction in heavy-duty milling machines," *Measurement*, vol. 128, pp. 34–44, Nov. 2018.
- [18] G. Kant and K. S. Sangwan, "Predictive modelling for energy consumption in machining using artificial neural network," *Procedia Cirp*, vol. 37, pp. 205–210, Jan. 2015.
- [19] W. Ming *et al.*, "Integrated ANN-LWPA for cutting parameter optimization in WEDM," *Int. J. Adv. Manuf. Technol.*, vol. 84, pp. 1277–1294, Sep. 2016.
- [20] G. Quintana, J. Ciurana, and J. Ribatallada, "Modeling power consumption in ball-end milling operations," *Adv. Manuf. Process.*, vol. 26, no. 5, pp. 746–756, 2011.
- [21] M. H. F. Al-Hazza, E. Y. T. Adesta, F. M. Ali, D. Agusman, and M. Y. Suprianto, "Energy cost modeling for high speed hard turning," *J. Appl. Sci.*, vol. 11, no. 14, pp. 2578–2584, 2011.
- [22] R. Bhinge, J. Park, K. H. Law, D. A. Dornfeld, M. Helu, and S. Rachuri, "Toward a generalized energy prediction model for machine tools," *J. Manuf. Sci. Eng.*, vol. 139, no. 4, 2017, Art. no. 041013.
- [23] T. Nguyen, "Prediction and optimization of machining energy, surface roughness, and production rate in SKD61 milling," *Measurement*, vol. 136, pp. 525–544, Mar. 2019.
- [24] Y. Han, J. Kim, and K. Lee, "Deep convolutional neural networks for predominant instrument recognition in polyphonic music," *IEEE/ACM Trans. Audio Speech.*, vol. 25, no. 1, pp. 208–221, Jan. 2017.

- [25] S. Yun, J. Choi, Y. Yoo, K. Yun, and J. Y. Choi, "Action-driven visual object tracking with deep reinforcement learning," *IEEE Trans. Neural Netw. Learn. Syst.*, vol. 29, no. 6, pp. 2239–2252, Jun. 2018.
- [26] T. Young, D. Hazarika, S. Poria, and E. Cambria, "Recent trends in deep learning based natural language processing [Review Article]," *IEEE Comput. Intell. Mag.*, vol. 13, no. 3, pp. 55–75, Aug. 2018.
- [27] V. T. Tran, F. Althobiani, and A. Ball, "An approach to fault diagnosis of reciprocating compressor valves using Teager-Kaiser energy operator and deep belief networks," *Expert Syst. Appl.*, vol. 41, no. 9, pp. 4113–4122, 2014.
- [28] R. Zhao, R. Yan, Z. Chen, K. Mao, P. Wang, and R. X. Gao, "Deep learning and its applications to machine health monitoring," *Mech. Syst. Signal Process.*, vol. 115, pp. 213–237, Jan. 2019.
- [29] X. Li, Q. Ding, and J.-Q. Sun, "Remaining useful life estimation in prognostics using deep convolution neural networks," *Rel. Eng. Syst. Saf.*, vol. 172, pp. 1–11, Apr. 2018.
- [30] D. Y. Pimenov, A. Bustillo, and T. Mikolajczyk, "Artificial intelligence for automatic prediction of required surface roughness by monitoring wear on face mill teeth," *J. Intell. Manuf.*, vol. 29, pp. 1045–1061, Jun. 2018.
- [31] Z. Jurkovic, G. Cukor, M. Brezocnik, and T. Brajkovic, "A comparison of machine learning methods for cutting parameters prediction in high speed turning process," *J. Intell. Manuf.*, vol. 29, pp. 1683–1693, Dec. 2018.
- [32] K. Amasyali and N. M. El-Gohary, "A review of data-driven building energy consumption prediction studies," *Renew. Sustain. Energy Rev.*, vol. 81, pp. 1192–1205, Jan. 2018.
- [33] C. Liu, Y. Li, G. Zhou, and W. Shen, "A sensor fusion and support vector machine based approach for recognition of complex machining conditions," *J. Intell. Manuf.*, vol. 29, no. 8, pp. 1739–1752, Dec. 2018.
- [34] X. Chen, C. Li, Y. Tang, and Q. Xiao, "An Internet of Things based energy efficiency monitoring and management system for machining workshop," *J. Clean. Prod.*, vol. 199, pp. 957–968, Oct. 2018.
- [35] T. Liu, W. Gao, Y. Tian, D. Zhang, Y. Zhang, and W. Chang, "Power matching based dissipation strategy onto spindle heat generations," *Appl. Therm. Eng.*, vol. 113, pp. 499–507, Feb. 2017.
- [36] T. Schudeleit, S. Züst, and K. Wegener, "Methods for evaluation of energy efficiency of machine tools," *Energy*, vol. 93, pp. 1964–1970, Dec. 2015.
- [37] X. Ma, "A brief introduction to the grey machine learning," *J. Grey Syst.*, vol. 31, no. 1, pp. 1–12, 2019.
- [38] C. E. Rasmussen and C. K. I. Williams, *Gaussian Processes for Machine Learning*. Cambridge, MA, USA: MIT Press, 2006.
- [39] A. Ferreira and G. Giraldi, "Convolutional neural network approaches to granite tiles classification," *Expert Syst. Appl.*, vol. 84, pp. 1–11, Oct. 2017.
- [40] G. Wang, J. Qiao, J. Bi, W. Li, and M. Zhou, "TL-GDBN: Growing deep belief network with transfer learning," *IEEE Trans. Autom. Sci. Eng.*, vol. 16, no. 2, pp. 874–885, Apr. 2019.
- [41] D. Hong, L. Baizano, and J. A. Fessier, "Asymptotic performance of PCA for high-dimensional heteroscedastic data," *J. Multivar. Anal.*, vol. 167, pp. 435–452, Sep. 2018.
- [42] C. Cui, M. Hu, J. D. Weir, and T. Wu, "A recommendation system for meta-modeling: A meta-learning based approach," *Expert Syst. Appl.*, vol. 46, pp. 33–44, Mar. 2016.
- [43] Y. Chen, H. Tan, and U. Berardi, "Day-ahead prediction of hourly electric demand in non-stationary operated commercial buildings: A clustering-based hybrid approach," *Energy Build.*, vol. 148, pp. 228–237, Aug. 2017.
- [44] S. Gao, M. Zhou, Y. Wang, J. Cheng, H. Yachi, and J. Wang, "Dendritic neuron model with effective learning algorithms for classification, approximation, and prediction," *IEEE Trans. Neural Netw. Learn. Syst.*, vol. 30, no. 2, pp. 601–614, Feb. 2019.
- [45] X. Ma, X. Mei, W. Wu, X. Wu, and B. Zeng, "A novel fractional time delayed grey model with grey wolf optimizer and its applications in forecasting the natural gas and coal consumption in chongqing china," *Energy*, vol. 178, pp. 487–507, Jul. 2019.
- [46] J. Wang and T. Kumbasar, "Parameter optimization of interval type-2 fuzzy neural networks based on PSO and BBBC methods," *IEEE/CAA J. Autom. Sinica*, vol. 6, no. 1, pp. 247–257, Jan. 2019.
- [47] J. Guo, L. Yang, R. Bie, J. Yu, Y. Gao, Y. Shen, and A. Kos, "An XGBoost-based physical fitness evaluation model using advanced feature selection and Bayesian hyper-parameter optimization for wearable running monitoring," *Comput. Netw.*, vol. 151, no. 1, pp. 166–180, Mar. 2019.
- [48] F. Kara, K. Aslantas, and A. Cicek, "ANN and multiple regression method-based modelling of cutting forces in orthogonal machining of AISI 316L stainless steel," *Neural Comput. Appl.*, vol. 26, no. 1, pp. 237–250, 2015.



Qinge Xiao (Member, IEEE) received the M.S. degree in industrial engineering from Chongqing University, Chongqing, China, in 2016, where she is currently pursuing the Ph.D. degree in mechanical engineering with a specialization in process modeling and intelligent optimization methods for sustainable manufacturing systems.

She has authored or coauthored ten technical articles in journals and conference proceedings.



Congbo Li (Senior Member, IEEE) received the B.S. and Ph.D. degrees from Chongqing University, Chongqing, China, in 2004 and 2009, respectively.

He is currently a Professor of mechanical engineering with Chongqing University. His research interests include modeling and optimization control, and energy-efficient manufacturing. His work has resulted in one book and over 100 journal and conference proceeding articles.

Dr. Li is currently serving as the Co-Chair for the IEEE Robotics and Automation Technical Committee on Sustainable Production Automation, a Guest Editor for Special Issue of the IEEE TRANSACTIONS ON AUTOMATION SCIENCE AND ENGINEERING, and *Robotics and Computer-Integrated Manufacturing*. He has chaired several technical sessions for IEEE conferences, including the Session of the IEEE CASE for Advances in Sustainable Production Automation and the Session of the IEEE SMC for Smart Energy Solutions to Sustainable Production Service and Automation.



Ying (Gina) Tang (Senior Member, IEEE) received the B.S. and M.S. degrees from Northeastern University, Shenyang, China, in 1996 and 1998, respectively, and the Ph.D. degree from the New Jersey Institute of Technology, Newark, NJ, USA, in 2001.

In 2002, she joined Rowan University, Glassboro, NJ, USA, where she is currently a Professor of electrical and computer engineering. Her research interests lie in modeling and control for computer-integrated systems, green manufacturing, and automation. Her work has resulted in over 150 publications, including one U.S. patent, two edited books, six book chapters, 41 journal articles, and over 100 conference proceeding articles.

Dr. Tang is currently serving as an Associate Editor for the IEEE TRANSACTIONS ON COMPUTATIONAL SOCIAL SYSTEMS, the *International Journal of Intelligent Control and Systems*, and the IEEE TRANSACTIONS ON AUTOMATION SCIENCE AND ENGINEERING, and an Editorial Board Member of the *International Journal of Remanufacturing*.



Xingzheng Chen (Member, IEEE) received the B.S. degree from North University of China, Taiyuan, China, in 2013, and the Ph.D. degree from Chongqing University, Chongqing, China, in 2018. He is currently a Lecturer with the College of Engineering and Technology, Southwest University, Chongqing. His research focuses on green manufacturing, energy efficiency machining, and system modeling and simulation. His work has resulted in over 15 publications, including ten journal articles, three conference proceeding articles, and three Chinese patents.